sustainability

Article

Trajectory Following Control of Modern Configurable Multi-Articulated Urban Bus Based on Model Predictive Control

Lu Shen and Liwei Zhang *

School of Electrical Engineering, Beijing Jiaotong University, Beijing 100044, China
* Correspondence: lwzhang@bjtu.edu.cn; Tel.: +86-158-0151-3998

Abstract: The configurable and multi-articulated urban bus is a new type of urban vehicle with the advantages of road vehicles and urban rail trains. However, its articulated and long body structure will bring about difficulties in steering control and trajectory following. Moreover, the following carriages easily deviate from their expected path, leading to the fishtailing and folding of the compartment. In this paper, we propose a generic framework that allows the rapid building of kinematic models for the new train. By introducing the MPC theory, we design a trajectory tracking controller for a multi-articulated vehicle with an arbitrary number of carriages. To verify our models, we establish kinematic models and a trajectory tracking controller for a multi-articulated train with different number of compositions in MATLAB. Under the double-lane-change track and serpentine road conditions, the trajectory tracking of the train is simulated. The influence of the number of carriages, velocity, and length of carriage on the trajectory tracking are further analyzed. The experimental results show the feasibility of our method. Our findings thus provide significant guidance for the design, actual configuration, and trajectory tracking control of the new multi-articulated urban bus.

Keywords: configurable urban bus; multi-articulated vehicle; trajectory following; model predictive control (MPC)

Citation: Shen, L.; Zhang, L. Trajectory Following Control of Modern Configurable Multi-Articulated Urban Bus Based on Model Predictive Control. *Sustainability* **2022**, *14*, 16619. https://doi.org/10.3390/su142416619

Academic Editors: Chao Sun, Dong Zhang, Xingyu Zhou and Filomena Mauriello

Received: 21 October 2022
Accepted: 6 December 2022
Published: 12 December 2022

1. Introduction

In recent years, the urban population has continued to grow with the rapid development of China's economy. However, due to the imbalance of supply and demand in urban traffic, the lagging of traffic development and supporting facilities, and the relatively backward construction of large-capacity rail transit [1], the problem of traffic congestion is becoming more and more serious. Urban public transport systems in large and medium-sized cities face enormous challenges in terms of efficiency and capacity.

The modern urban bus is a new type of urban vehicle. It has the advantages of flexible operation, low infrastructure cost, large capacity, and flexible formation similar to urban rail trains. Therefore, it is an excellent supplement to the existing urban transportation system and the focus of the future development of urban transportation. The train consists of driver, trailer, and power modules interconnected with passive rotary joints. It has the function of multi-axle steering, which can significantly decrease the turning radius and improve the flexibility of the train in complex driving conditions.

However, the bus's articulated and long body structure brings about difficulties in steering control and increases the area of road occupied when turning. Moreover, the following carriages easily deviate from the expected driving path, leading to the tail swing and folding of the compartment. Therefore, it is necessary to study the trajectory tracking control of the modern urban bus.

The tracking self-guiding system of the vehicle mainly includes two parts: the pose perception system and the trajectory following control system. Since modern urban buses share the right of way with ordinary vehicles on urban roads, they will interact with other vehicles during actual operation. The pose sensor of the vehicle body detects the surrounding environment information of the vehicle while acquiring the pose information of the vehicle. It transmits the data to the trajectory following control system after data fusion. Therefore, based on the known environmental information and pose information, it is a problem to be solved to ensure that the modern urban bus runs on its predetermined trajectory.

A kinematic model of the multi-articulated urban bus is very important in the rapid planning of nominal maneuvering, vehicle motion prediction, low-speed maneuvering control, and driver assistance design [2]. Therefore, it is necessary to establish a kinematic model. However, the current research on the kinematic modeling of articulated vehicles is mainly focused on special vehicles with a limited number of trucks or compartments, such as single articulated vehicles [3], underground mining articulated vehicles [4], and double articulated vehicles [5,6]. For multi-articulated vehicles, the research mainly focuses on the N-trailer vehicle, which is usually equipped with fixed truck wheels. Michalek proposed a modular modeling approach that allows the construction of a compact nonholonomic kinematic model of a multi-articulated bus consisting of a tractor and N wagons with fixed or steerable wheels [2].The trajectory following problem of the modern urban bus is a highly nonlinear optimization problem with multi-joint constraints, and the joint coupling between multi-body systems increases the nonlinearity and complexity of the model, which affects the difficulty of controller design [7]. There are few studies on the trajectory following problem of multi-articulated urban buses. The current control methods mainly include traditional feedback control, optimal control, intelligent control, etc. [8–10].

Reference [11] proposed a trajectory following feedback control strategy for a coupled vehicle with five axles and three steering axles, and the control effect was verified through experiments. A. Astolfi et al. [12] established a trajectory compensation model for an articulated semi-trailer and designed a trajectory following controller for straight and circular trajectories. This solved the problem of steering limitations of corner saturation. For the tracking control of any trajectory, Mitsuji Sampei [13] took the distance traveled by the vehicle along the desired trajectory as the time scale and used the precise feedback linearization method to design a path-tracking controller for articulated vehicles. This study achieved good results in the backward-moving eight-shaped path-following control experiment.

With the continuous development of computer technology and control theory, intelligent algorithms have been increasingly used in trajectory following control in recent years, for example, fuzzy control algorithms, neural network algorithms, and genetic algorithms, etc. [14–16]. Because the traditional PID control algorithm is sensitive to working conditions and has poor robustness when solving complex trajectory following control problems, fuzzy algorithms and neural network algorithms are often used to optimize PID parameters. Reference [17] designed a fuzzy PID controller for the trajectory following system of an articulated tracked vehicle. The PID parameters were optimized through the fuzzy controller, and the vehicle had fast and accurate tracking performance under straight and curved road conditions. Reference [18] proposed a genetic algorithm to optimize the weight matrix of LQR to realize the stable trajectory following control of articulated vehicles. Reference [19] used the genetic particle algorithm to optimize the weight coefficient of the LQR control algorithm and improve the optimization operation speed; the study switched the weight coefficient according to different working conditions to achieve the followability and driving stability of the articulated semi-trailer.

The intelligent control method has self-learning and adaptive functions, but it has not yet been maturely applied in the field of trajectory following control. The optimal control is simple in design and suitable for solving multi-input and multi-output problems. The most commonly used method of optimal control in trajectory following control is LQR (Linear Quadratic Regulator) control and MPC (Model Predictive Control) control [20,21]. Reference [22] proposed a double-closed-loop trajectory following control method for articulated semi-trailers, using a highly robust sliding mode control as the dynamic speed controller. The study proved that the combination of MPC and sliding mode control had better tracking and smaller tracking error than the combination of LQC and sliding mode control. Reference [23] adopted the yaw rate based MPC control to suppress road curvature disturbance and proposed a vehicle sideslip compensator to correct the predictive model. Compared with traditional feedback control, optimal control has the advantages of simple design and strong robustness; compared with LQR control, MPC control has more control advantages.

The two main contributions of this paper are as follows:

(1) This paper proposes a general framework to quickly construct a kinematic model of a new type of modern urban bus. Unlike traditional N trailers, this train has a completely new structure. It consists of two drive modules with steering shafts and any number of independent power modules and wheelless trailer modules, which are interconnected by passive swivel joints. The trailer module and power module can be combined flexibly according to the passenger capacity.
(2) Based on the kinematic model, by introducing the MPC model a trajectory tracking controller for a multi-articulated vehicle with an arbitrary number of carriages is designed, and the influences of the number of carriages, velocity, and length of carriage on the trajectory tracking are further analyzed.

As far as the author knows, it is the first time relevant analysis on the modern urban buses with the above-mentioned structure has been undertaken.

The rest of the paper is structured as follows: Section 2 presents the structure and kinematics model of the novel configurable multi-articulated urban bus, Section 3 presents the proposed MPC-based train trajectory tracking strategy, Section 4 presents the simulation results for different train combinations, and Section 5 summarizes the paper's contributions and discusses directions for future work.

2. Modern Configurable Multi-Articulated Urban Bus

2.1. Structure of the Train

The modern urban bus is an articulated and configurable trackless self-guided rubber-tired trolley bus. The whole train adopts a 100% low-floor structure, which makes it convenient for passengers to get on and off the train. The train is composed of driver modules (DM), trailer modules (TM), and central modules (CM). Driver modules are situated at both ends of the train, which allow the train to travel in both directions.

The driver module is equipped with a non-power running gear composed of a steering axle. The central module is equipped with a power running gear composed of two hub motors to provide driving power. The trailer module is without running gear; its supporting force is provided by the adjacent central modules. The trailer modules and power modules can be grouped flexibly according to passenger volume; this also allows the train to meet the transportation needs of different passenger flows and minimize the energy consumption of transportation. The modules are connected by articulations composed of a fixed hinge, an elastic hinge, and a free hinge. The yaw motion of the train is mainly realized by the fixed hinges. The structure of the train is shown in Figure 1.

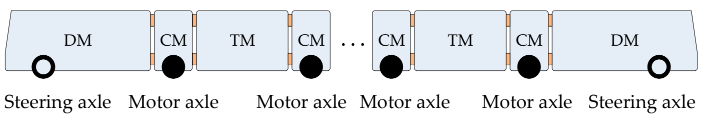

Figure 1. Structure of the modern configurable multi-articulated urban bus.

The steering system of the train is mainly composed of two parts:

(1) Electric power steering of the head driver module and adaptive steering of the rear driver module.
(2) The central module realizes the steering by controlling the speed difference between the two hub motors. The train is equipped with a self-guided tracking system composed of a position and attitude perception system and a trajectory tracking control system. The perception system obtains the current train posture information through a

differential global positioning system (GPS), LIDARs, monocular cameras, and inertial measurement units (IMUs). The trajectory tracking control system gives the steering commands according to the vehicle position, its posture information, the driver's steering wheel angle, and the driving throttle information to realize the coordinated steering of the train and keep the train running on its expected path.

2.2. Kinematic Models of the Train

As the modern urban bus is mainly designed to run on urban roads with good road conditions and at low speed, the modeling proposed in the sequel is built on the following assumptions:

(1) The impact of the elastic deformation on the axial direction of the tire is ignored. That is, the tires do not produce sideslip motion.
(2) All the wheels rotate without skid and/or slip effects.
(3) Only the planar motion of the vehicles is considered. That is, roll and pitch degrees of freedom are neglected.
(4) All the vehicle's bodies are rigid.
(5) Considering that the central module is much smaller than the driver and trailer modules, the train is further equivalent to the structure shown in Figure 2.

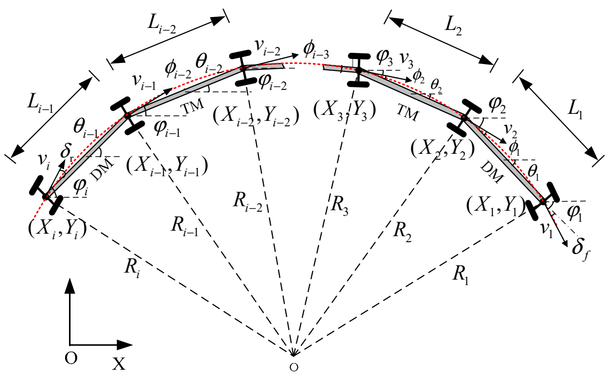

Figure 2. Schematic diagram of the modern urban bus.

Considering that the trailer and central modules can be grouped flexibly according to passenger volume, assume that a train contains two driver modules, $i-2$ central modules, and $i-3$ trailer modules. The kinematic models of the train are established in the XOY global coordinate frame. Assume that the Ackerman steering condition has been met and that point o is the instantaneous steering center of the train.

The coordinates of the center of *Axle i* is (X_i, Y_i), the yaw angle of *Axle i* is φ_i, in radians; δ_f and δ_r are the equivalent steering angles of the head and tail axle, respectively. ϕ_j is the articulation angle between the $j+1$ axle and the carriage j, in radians. v_i is the velocity of *Axle i*, in m/s; L_i is the length of the carriage; the yaw angle of carriage i is θ_i, in radians.

Based on the geometric relationship of the carriages, the following constraints are met:

$$\begin{cases} X_{j+1} = X_j - L_j \cdot \cos\theta_j \\ Y_{j+1} = Y_j - L_j \cdot \sin\theta_j \end{cases}, j = 1, 2, \cdots, i-1 \tag{1}$$

Since the rigid body does not consider deformation, the following constraints are met:

$$\begin{cases} v_2 \cdot \cos(\phi_1) = v_1 \cdot \cos\delta_f \\ v_{j+2} \cdot \cos(\phi_{j+1}) = v_{j+1} \cdot \cos(\theta_{j+1} - \theta_j - \phi_j), j = 1, 2, \cdots i-3 \\ v_i \cdot \cos(\delta_r) = v_{i-1} \cdot \cos(\theta_{i-1} - \theta_{i-2} - \phi_{i-2}) \end{cases} \tag{2}$$

According to Figure 2, the yaw angles and the articulation angles meet the following constraints:

$$\begin{cases} \varphi_1 = \theta_1 + \delta_f \\ \varphi_{j+1} = \theta_j + \phi_j, j = 1, 2, \cdots, i-2 \\ \varphi_i = \theta_{i-1} + \delta_r \end{cases} \tag{3}$$

Set the velocity of the first axle as the driver's expected velocity, decompose the speed of each axle along the X-axis and Y-axis, and substitute (3), then we can obtain the state equations for each axle.

$$\begin{cases} \dot{X}_1 = v_1 \cdot \cos(\theta_1 + \delta_f) \\ \dot{Y}_1 = v_1 \cdot \sin(\theta_1 + \delta_f) \\ \dot{X}_{j+1} = v_{j+1} \cdot \cos(\theta_j + \phi_j) \\ \dot{Y}_{j+1} = v_{j+1} \cdot \sin(\theta_j + \phi_j) \\ \dot{X}_\mathrm{i} = v_i \cdot \cos(\theta_{i-1} + \delta_r) \\ \dot{Y}_i = v_i \cdot \sin(\theta_{i-1} + \delta_r) \end{cases}, j = 1, 2, \cdots, i-2 \tag{4}$$

By analyzing the velocity at both ends of the carriage, we can obtain the yaw rate of the carriage:

$$\begin{cases} \dot{\theta}_1 = (v_1 \cdot \sin(\delta_f) - v_2 \cdot \sin(\phi_1))/L_1 \\ \dot{\theta}_{j+1} = (-v_{j+1} \cdot \sin(\theta_{j+1} - \theta_j - \phi_j) - v_{j+2} \cdot \sin(\phi_{j+1}))/L_{j+1}, j = 1, 2, \cdots, i-3 \\ \dot{\theta}_{i-1} = (-v_{i-1} \cdot \sin(\theta_{i-1} - \theta_{i-2} - \phi_{i-2}) - v_i \cdot \sin(\delta_r))/L_{i-1} \end{cases} \tag{5}$$

The central module is driven by two hub motors and adopts the differential speed control system to realize module steering. Therefore, the rate of the yaw angle and the velocities of the wheels meet the following constraints:

$$\dot{\varphi}_{j+1} = \frac{v_{j+1R} - v_{j+1L}}{D_{j+1}}, j = 1, 2, \cdots, i-2 \tag{6}$$

where D is the wheelbase of the axle, in meter. v_R and v_L are the velocities of the left and right wheel of the same axle, respectively; and they meet the following constraints:

$$v_j = \frac{v_{jR} + v_{jL}}{2} \tag{7}$$

According to (4) and (5), the kinematic models of the modern urban bus can be obtained.

2.3. Linearization and Discretization of the Model

Since the kinematic model of the train is a non-linear and time-varying system, linearization and discretization are required to improve the real-time performance of the system. Take x and u as the state variable and controlled variable, respectively. The state equations of the train can be abbreviated as follow:

$$\dot{x} = f(x, u) \tag{8}$$

where $x = (X, Y, \theta)^T$; $u = (\delta_f, \Phi, \delta_r)^T$.

Assume that the train can completely pass the expected path. That is, each point on the expected path satisfies the kinematic equations of the train, and the kinematic models can be linearized by the error between the reference and actual state of the train. The reference state and controlled variables of the train at any time satisfy (9).

$$\dot{x}_r = f(x_r, u_r) \tag{9}$$

Performing Taylor expansion of the state equations at the reference point, we can obtain the system's continuous linearized state equations.

$$\dot{\widetilde{x}} = A(t) \cdot \widetilde{x} + B(t) \cdot \Delta u \tag{10}$$

where $\widetilde{x} = x - x_r$, $\Delta u = u - u_r$, $A(t)$ and $B(t)$ are the Jacobian matrixes of function f with respect to x and u, respectively.

Suppose the sampling period is T_s, and (10) can be discretized:

$$\widetilde{x}(k+1) = A_{k,t}\widetilde{x}(k) + B_{k,t}\Delta u(k) \tag{11}$$

where $A_{k,t} = 1 + T_s A(t)$, $B_{k,t} = T_s B(t)$.

According to the state equations of the train, specific expressions can be further obtained by (12) and (13).

$$A_{k,t} = \begin{bmatrix} E_{2i\times 2i} & a_{2i\times(i-1)} \\ 0_{(i-1)\times 2i} & b_{(i-1)\times(i-1)} \end{bmatrix} \tag{12}$$

$$B_{k,t} = \begin{bmatrix} c_{2i\times i} \\ d_{(i-1)\times i} \end{bmatrix} \tag{13}$$

where $E_{2i\times 2i}$ is an identity matrix; $0_{(i-1)\times 2i}$ is a zero matrix, and $a_{2i\times(i-1)}$, $b_{(i-1)\times(i-1)}$, $c_{2i\times i}$ and $d_{(i-1)\times i}$ are shown as below.

$$\left\{ \begin{aligned}
a_{2i\times(i-1)} &= \begin{bmatrix}
-v_1 \cdot \sin(\theta_1+\delta_f)*\mathrm{T} & 0 & 0 & 0 & 0 \\
v_1 \cdot \cos(\theta_1+\delta_f)*\mathrm{T} & 0 & 0 & 0 & 0 \\
-v_2 \cdot \sin(\theta_1+\phi_1)*\mathrm{T} & 0 & 0 & 0 & 0 \\
v_2 \cdot \cos(\theta_1+\phi_1)*\mathrm{T} & 0 & 0 & 0 & 0 \\
0 & \ddots & 0 & 0 & 0 \\
0 & \ddots & 0 & 0 & 0 \\
0 & 0 & -v_{j+1} \cdot \sin(\theta_j+\phi_j)*\mathrm{T} & 0 & 0 \\
0 & 0 & v_{j+1} \cdot \cos(\theta_j+\phi_j)*\mathrm{T} & 0 & 0 \\
0 & 0 & 0 & \ddots & 0 \\
0 & 0 & 0 & \ddots & 0 \\
0 & 0 & 0 & 0 & -v_i \cdot \sin(\theta_{i-1}+\delta_r)*\mathrm{T} \\
0 & 0 & 0 & 0 & v_i \cdot \cos(\theta_{i-1}+\delta_r)*\mathrm{T}
\end{bmatrix} \\
b_{(i-1)\times(i-1)} &= \begin{bmatrix}
1 & v_2 \cdot \cos(\theta_2-\theta_1-\phi_1)*\mathrm{T}/L_2 & 0 & 0 & 0 \\
0 & 1 - v_2 \cdot \cos(\theta_2-\theta_1-\phi_1)*\mathrm{T}/L_2 & \ddots & 0 & 0 \\
0 & 0 & \ddots & \ddots & 0 \\
0 & 0 & & 1 - v_{j+1} \cdot \cos(\theta_{j+1}-\theta_j-\phi_j)*\mathrm{T}/L_{j+1} & v_{j+2} \cdot \cos(\theta_{j+2}-\theta_{j+1}-\phi_{j+1})*\mathrm{T}/L_{j+2} \\
0 & 0 & 0 & 0 & 1 - v_{j+2} \cdot \cos(\theta_{j+2}-\theta_{j+1}-\phi_{j+1})*\mathrm{T}/L_{j+2}
\end{bmatrix}^{\mathrm{T}} \\
c_{2i\times i} &= \begin{bmatrix}
-v_1 \cdot \sin(\theta_1+\delta_f)*\mathrm{T} & 0 & 0 & 0 & 0 \\
v_1 \cdot \cos(\theta_1+\delta_f)*\mathrm{T} & 0 & 0 & 0 & 0 \\
0 & \ddots & 0 & 0 & 0 \\
0 & \ddots & 0 & 0 & 0 \\
0 & 0 & -v_{j+1} \cdot \sin(\theta_j+\phi_j)*\mathrm{T} & 0 & 0 \\
0 & 0 & v_{j+1} \cdot \cos(\theta_j+\phi_j)*\mathrm{T} & 0 & 0 \\
0 & 0 & 0 & \ddots & 0 \\
0 & 0 & 0 & \ddots & 0 \\
0 & 0 & 0 & 0 & -v_{i-1} \cdot \sin(\theta_{i-2}+\delta_r)*\mathrm{T} \\
0 & 0 & 0 & 0 & v_{i-1} \cdot \cos(\theta_{i-2}+\delta_r)*\mathrm{T}
\end{bmatrix} \\
d_{(i-1)\times i} &= \begin{bmatrix}
v_1 \cdot \cos(\delta_f)*\mathrm{T}/L_1 & -v_2 \cdot \cos(\phi_1)*\mathrm{T}/L_1 & 0 & 0 & 0 & 0 & 0 \\
0 & v_2 \cdot \cos(\theta_2-\theta_1-\phi_1)*\mathrm{T}/L_2 & -v_3 \cdot \cos(\phi_2)*\mathrm{T}/L_2 & 0 & 0 & 0 & 0 \\
0 & 0 & \ddots & -v_{j+1} \cdot \cos(\phi_j)*\mathrm{T}/L_j & 0 & 0 & 0 \\
0 & 0 & 0 & v_{j+1} \cdot \cos(\theta_{j+1}-\theta_j-\phi_j)*\mathrm{T}/L_{j+1} & \ddots & 0 & 0 \\
0 & 0 & 0 & 0 & \ddots & -v_{i-1} \cdot \cos(\phi_{i-2})*\mathrm{T}/L_{i-2} & 0 \\
0 & 0 & 0 & 0 & 0 & v_{i-1} \cdot \cos(\theta_{i-1}-\theta_{i-2}-\phi_{i-2})*\mathrm{T}/L_{i-1} & -v_i \cdot \cos(\delta_r)*\mathrm{T}/L_{i-1}
\end{bmatrix}
\end{aligned} \right.$$

Therefore, for a modern urban bus with an arbitrary number of carriages, the linear and discrete kinematic models can be directly obtained by (11)–(13), which can be taken as the predictive model for trajectory tracking control.

3. Trajectory Following Strategy of Modern Urban Bus Based on MPC

According to the state equations of the train, we know that by controlling the steering and articulation angles for a given path and velocity of the train, the train can be driven on the expected path. Since the urban bus is a multi-input, multi-output, and multi-constrained system, we introduced the MPC method to optimize the control target of the train to achieve the trajectory following.

The MPC model mainly included three key parts [15]: predictive model, rolling optimization, and feedback correction. It established a predictive model to predict the future controlled variables and system states and then solved the optimization problem under the condition that the objective function and various constraints were satisfied. The optimization process could be repeated online as the sampling time went on to obtain a series of optimally controlled variables in the control time domain.

In this paper, we took the yaw angles' deviation of the train as the controlled objective and established a predictive model based on the discretization model to determine the optimal objective at each moment. Then we took the optimal control value as input at the next moment. The principle of the MPC-based trajectory following controller is shown in Figure 3.

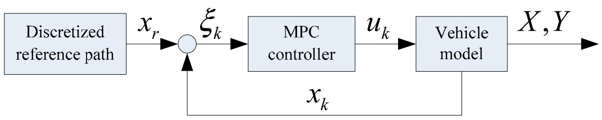

Figure 3. Principle of MPC-based trajectory following.

3.1. Construction of the Target Trajectory

When a vehicle is running, the trajectory is an irregular curve that can be regarded as a combination of curves with different curvatures. The trajectory of the modern urban bus is shown as Figure 4. The driver needs to adjust the steering angle of the vehicle according to the road conditions.

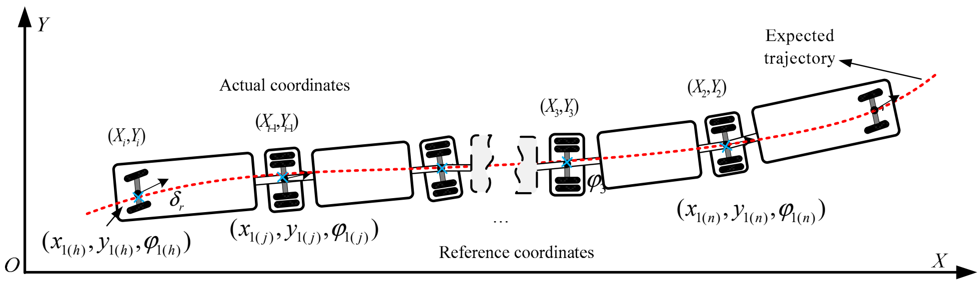

Figure 4. Trajectory of the modern urban bus.

As the first axle of the vehicle is controlled by the driver, the steering angle of the first axle is generally given by a driver model, such as the optimal preview model. The vehicle control system controls the steering angle of the trailing car and the articulation angles of the intermediate ones to ensure that the vehicle follows the trajectory of the first axle. As the driver model is not the focus of this paper, for the sake of simplification, we ignored the driver model and assumed that the driver could adjust the steering angle of the first axle completely according to the expected path. The steering angle of the first axle is given according to the path directly.

Take the position of the first axle as the guide point of the trajectory and collect and store its position and yaw angle as the trajectory information of the train. As time goes by, the train continues to move forward, new coordinate values are stored, and the oldest stored ones are discarded. For this reason, a shift register is introduced. The process can be described as follow:

$$\begin{cases} x(k+1) = Ex(k) + Fx(1) \\ y(k+1) = Ey(k) + Fy(1) \\ \varphi(k+1) = E\varphi(k) + F\varphi(1) \\ s(k+1) = Es(k) + Fs(1) \end{cases} \tag{14}$$

where: E is a $(n+1) \times (n+1)$ matrix and F is a $(n+1) \times 1$ matrix. And $E = \begin{bmatrix} 0 & I_n \\ 0 & 0 \end{bmatrix}$, $F = (0, 0, \ldots, 0, 1)^T$.

3.2. Predictive Model Establishment

The predictive model is the basis of the MPC controller. The predictive model predicts the posture information of the train in the future by analyzing its current posture information and the control amount of the system. According to (11), the state space is reconstructed at time k and the predictive model is given by (15).

$$\begin{aligned} &\xi(k+1|t) = \widetilde{A}_{k,t} \cdot \xi(k|t) + \widetilde{B}_{k,t} \cdot \Delta u(k|t) \\ &\eta(k|t) = \widetilde{C}_{k,t}\xi(k|t) \end{aligned} \tag{15}$$

where $\xi(k|t) = \begin{bmatrix} x(k|t) \\ u(k-1|t) \end{bmatrix}, \widetilde{A}_{k,t} = \begin{bmatrix} A_{k,t} & B_{k,t} \\ 0_{m\times n} & I_m \end{bmatrix},$
$\widetilde{B}_{k,t} = \begin{bmatrix} B_{k,t} \\ I_m \end{bmatrix}, \widetilde{C}_{k,t} = [C_{k,t}, 0]$

Assume that the prediction time domain of the model is N_p, and the control time domain is N_c. The state variables and output of the system in the prediction time domain can be obtained by (16).

$$\begin{aligned} &\widetilde{\xi}(t+N_p|t) = \widetilde{A}_t^{N_p} \cdot \widetilde{\xi}(t/t) + \widetilde{A}_t^{N_p-1}\widetilde{B}_t \cdot \Delta u(t|t) + \cdots + \widetilde{A}_t^{N_p-N_c-1}\widetilde{B}_t \cdot \Delta u(t+N_c|t) \\ &Y(t) = \psi_t \cdot \widetilde{\xi}(t/t) + \Theta_t \cdot \Delta U(t|t) \end{aligned} \tag{16}$$

where

$$\widetilde{A}_{k,t} = \widetilde{A}_t, \widetilde{B}_{k,t} = \widetilde{B}_t, Y(t) = \left[\eta(t+1|t), \eta(t+2|t), \cdots, \eta(t+N_c|t), \cdots, \eta(t+N_p|t)\right]^T,$$

$$\psi_t = \left[\widetilde{C}_t\widetilde{A}_t, \widetilde{C}_t\widetilde{A}_t^2, \cdots, \widetilde{C}_t\widetilde{A}_t^{N_c}, \cdots, \widetilde{C}_t\widetilde{A}_t^{N_p}\right]^T,$$

$$\Delta U(t|t) = [\Delta u(t|t), \Delta u(t+1|t), \cdots, \Delta u(t+N_c|t)]^T$$

$$\Theta_t = \begin{bmatrix} \widetilde{C}_t\widetilde{B}_t & 0 & 0 & 0 \\ \widetilde{C}_t\widetilde{A}_t\widetilde{B}_t & \widetilde{C}_t\widetilde{B}_t & 0 & 0 \\ \cdots & \cdots & \ddots & \cdots \\ \widetilde{C}_t\widetilde{A}_t^{N_c-1}\widetilde{B}_t & \widetilde{C}_t\widetilde{A}_t^{N_c-2}\widetilde{B}_t & \cdots & \widetilde{C}_t\widetilde{B}_t \\ \widetilde{C}_t\widetilde{A}_t^{N_c}\widetilde{B}_t & \widetilde{C}_t\widetilde{A}_t^{N_c-1}\widetilde{B}_t & \cdots & \widetilde{C}_t \\ \vdots & \vdots & \ddots & \vdots \\ \widetilde{C}_t\widetilde{A}_t^{N_p-1}\widetilde{B}_t & \widetilde{C}_t\widetilde{A}_t^{N_p-2}\widetilde{B}_t & \cdots & \widetilde{C}_t\widetilde{A}_t^{N_p-N_c-1}\widetilde{B}_t \end{bmatrix}$$

In each control cycle, the coefficient matrix of the state variables is updated at time k as the optimal control input is recalculated, which in turn leads to the recalculation of the optimization problem to obtain a new optimal control sequence. This process is called rolling optimization, which always achieves the best control effect in the prediction time domain.

3.3. Objective Function and Optimization

Due to the incremental jump of the control quantity in each sampling period of the discrete system, chattering will occur during the driving process of the trackless vehicle, resulting in changes in the heading angle of each carriage and the articulation angle between carriages, which in turn reduces the stability of path tracking. Therefore, we adopted the error of the state variables and the control increment as the optimization objectives and limited the increment reasonably in this paper. The objective function is given as follows:

$$J(\widetilde{\xi}(t), u(t-1), \Delta U(t)) = \sum_{i=1}^{N_p} \|\xi(t+i/t) - \xi_{ref}(t+i/t)\|_Q^2 + \sum_{i=1}^{N_c-1} \|\Delta U(t+i)|t\|_R^2 + \rho\varepsilon^2 \tag{17}$$

where Q is the error weight matrix; R is the weight matrix of controlled variables; ρ is the weight matrix of the relaxation factors; ε is the matrix of relaxation factors.

The first term of (17) reflects the vehicle's ability to track the reference trajectory, and the second term reflects the requirement for smooth changes in the controlled variables. For a time-varying system, the introduction of the relaxation factors ensures a feasible solution of the optimization problem at each time.

To convert the objective function into a standard quadratic form, we introduce the output deviation in the forecast time domain:

$$E(t) = \psi_t \cdot \widetilde{\xi}(t/t) - Y_{ref}(t) \tag{18}$$

Combining the above equations, the final optimization objective function is obtained:

$$J(\widetilde{\xi}(t), u(t-1), \Delta U(t)) = \frac{1}{2}\left[\Delta U(t)^T, \varepsilon\right]^T H_t \left[\Delta U(t)^T, \varepsilon\right] + G_t \left[\Delta U(t)^T, \varepsilon\right] + P_t \tag{19}$$

where $H_t = diag\{2\Theta_t{}^T Q \Theta_t + R, 1\}$, $G_t = \left[2E(t)^T Q \Theta_t, 0\right]$, $P_t = E(t)^T Q E(t)$.

Therefore, the optimization problem is equivalent to solving the following quadratic programming problem:

$$\begin{aligned} &\min_{\Delta U_t, \varepsilon} \left[\Delta U(t)^T, \varepsilon\right]^T H_t \left[\Delta U(t)^T, \varepsilon\right] + G_t \left[\Delta U(t)^T, \varepsilon\right] \\ &s.t. \begin{cases} \Delta U_{\min} \le \Delta U(k) \le \Delta U_{\max} \\ U_{\min} \le U(t-1) + \sum\limits_{i=1}^{k} \Delta U(i) \le U_{\max} \\ Y_{\min} + \varepsilon \le \psi_t \cdot \xi(t/t) + \Theta_t \cdot \Delta U(t) \le Y_{\max} + \varepsilon, \varepsilon > 0 \end{cases} \end{aligned} \tag{20}$$

where $k = t, \ldots, t + N_c - 2, t + N_c - 1$

$(\Delta U_{\min}, \Delta U_{\max})$ is the constraint range of the input increment;

$(U_{\min}, U_{\max})$ is the constraint range of the input of the kinematic system;

$(Y_{\min}, Y_{\max})$ is the output constraint range of the system kinematics model.

By solving (20), we obtain the sequence of the controlled variables' increments in the control time domain of the kth control cycle:

$$\Delta U_k^* = [\Delta u_k^*, \Delta u_{k+1}^*, \Delta u_{k+2}^*, \cdots, \Delta u_{k+N_c-1}^*] \tag{21}$$

where Δu_k^* is the increment of the controlled variables at kth moment.

The first element in the sequence is input into the system as the actual control increment, that is:

$$u(k+1) = u(k) + \Delta u_k^* \tag{22}$$

In this way, we obtain the value of the controlled variables at the next moment and input it into the kinematic models of the train. The control process is shown in Figure 5. Repeat the above process to control the vehicle to follow the expected trajectory.

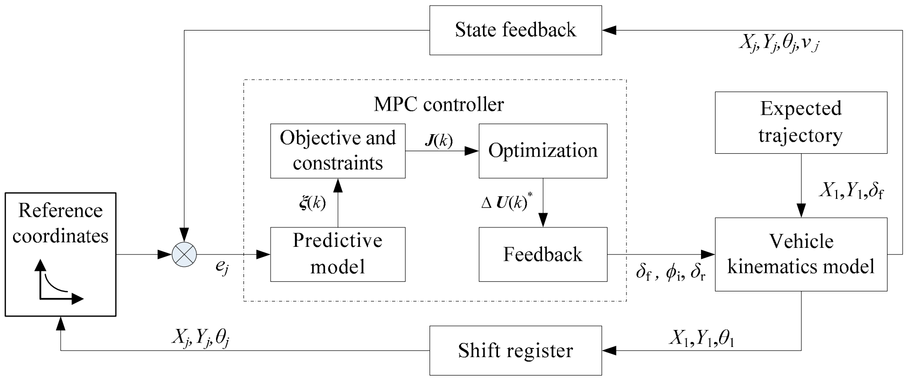

Figure 5. Schematic diagram of MPC-based trajectory following.

4. Simulation Analysis

To verify the models proposed in this paper, we established kinematical vehicle models and a trajectory-following controller based on MPC in MATLAB. And under double lane-change track and serpentine road conditions, the trajectory following the train was simulated.

To reflect the different configurations of the train, we established kinematic models for three kinds of trains in this paper, as shown in Figure 6, which are three-carriages with four-axles, four-carriages with five-axles, and five-carriages with six-axles trains. The wheel tread was 2.6 m, the equivalent length of a cab was 7 m, and the equivalent length of a carriage was 7 m.

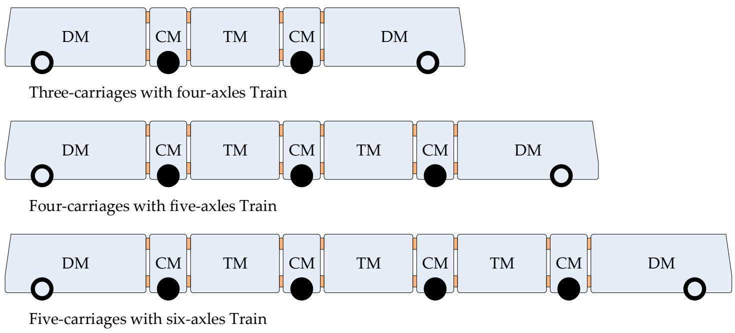

Figure 6. Train with different configurations.

4.1. Simulation Road Conditions

(1) Double lane-change track

The double lane-change track is one of the commonly used test tracks to analyze the stability and tracking performance of a car, which simulates the process of a car changing lanes, overtaking at a certain speed, and then returning to the original lane. Based on ISO 3888-1 [19], the dimensions of the double lane-change track are shown in Figure 7

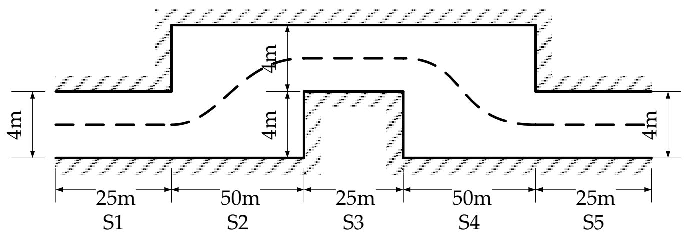

Figure 7. Double lane-change track.

The mathematical expression of the double lane-change track was fitted with a third-order polynomial as follow [20]:

$$\begin{cases} y = 0 & x \in [0, 25) \\ y = 6 - 0.54x + 0.0144x^2 - 0.000096x^3 & x \in [25, 75) \\ y = 6 & x \in [75, 100) \\ y = -162 + 4.32x - 0.036x^2 + 0.000096x^3 & x \in [100, 150) \\ y = 0 & x \in [150, 200) \end{cases} \tag{23}$$

The fitted path and its curvature are shown in Figures 8 and 9, respectively.

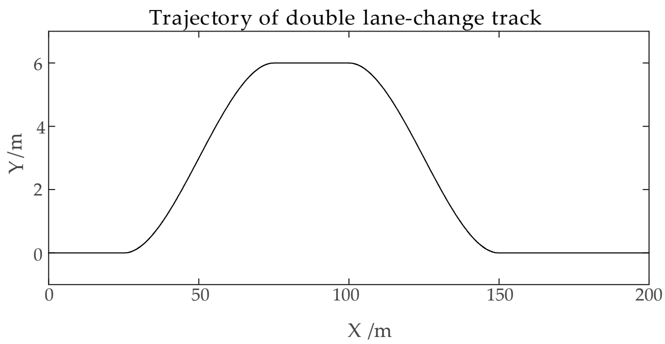

Figure 8. Trajectory of double lane-change track.

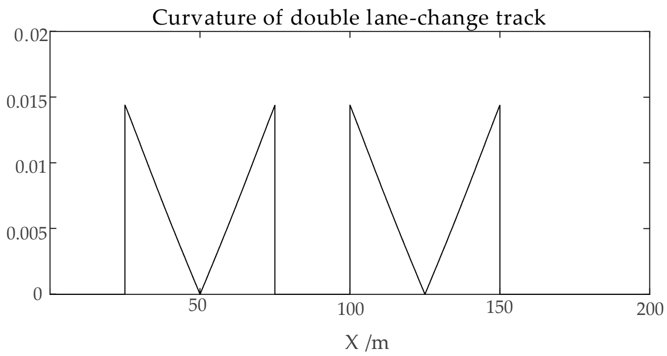

Figure 9. Curvature of double lane-change track.

(2) Serpentine track

The serpentine track is widely used in the pylon course slalom test, which tests the obstacle avoidance ability of the vehicle. Based on GB/T6323-2014 [24], the dimensions of the track are shown in Figure 10. According to the geometric dimensions of modern urban bus, the pile distance was set to 50 m. The mathematical expression of the track was fitted with a trigonometric function as follows [25]:

$$\begin{cases} y = 0 & x \in [0, 25) \\ y = 3(1 - \cos(\frac{(x-25)}{25} * pi)) & x \in [25, 50) \\ y = 6\cos(\frac{(x-50)}{50} * pi) & x \in [50, 300) \\ y = -3(1 + \cos(\frac{(x-300)}{25} * pi)) & x \in [300, 325) \\ y = 0 & x \in [325, 400) \end{cases} \tag{24}$$

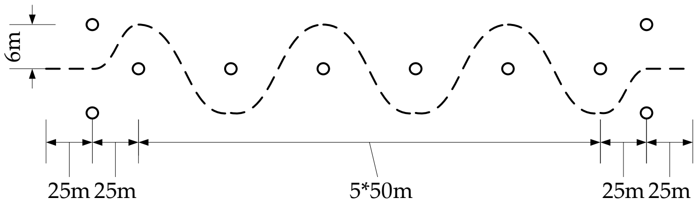

Figure 10. Serpentine track.

The fitted path and its curvature are shown in Figures 11 and 12, respectively.

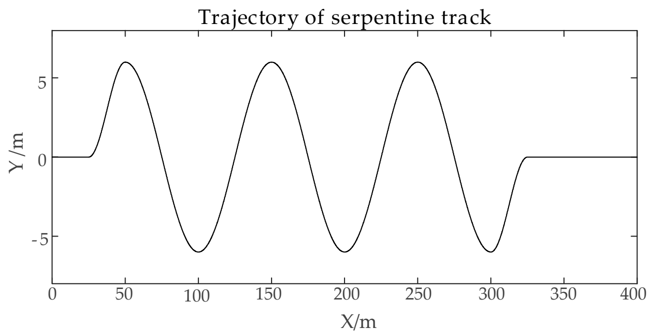

Figure 11. Trajectory of serpentine track.

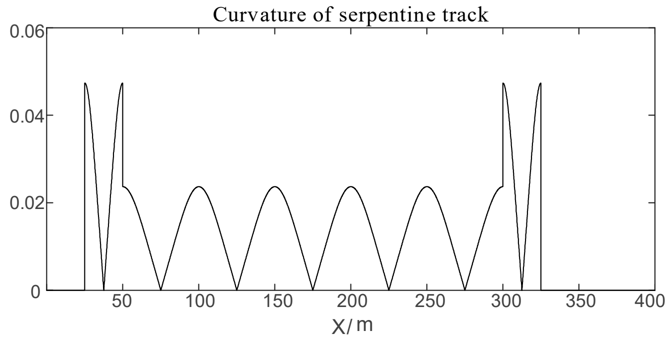

Figure 12. Curvature of serpentine track.

4.2. Simulation Results

Under the double lane-change condition, the trajectories of each axle and the trajectory-following error of the train with different configurations are shown in Figures 13 and 14.

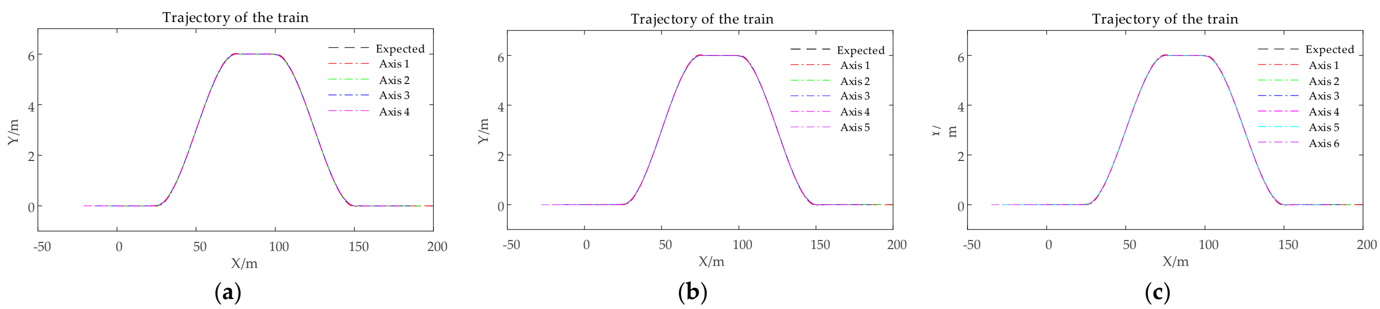

Figure 13. Trajectories of each axle of the train with different configurations. (**a**) Three-carriages with four-axles train; (**b**) Four-carriages with five-axles train; (**c**) Five-carriages with six-axles train.

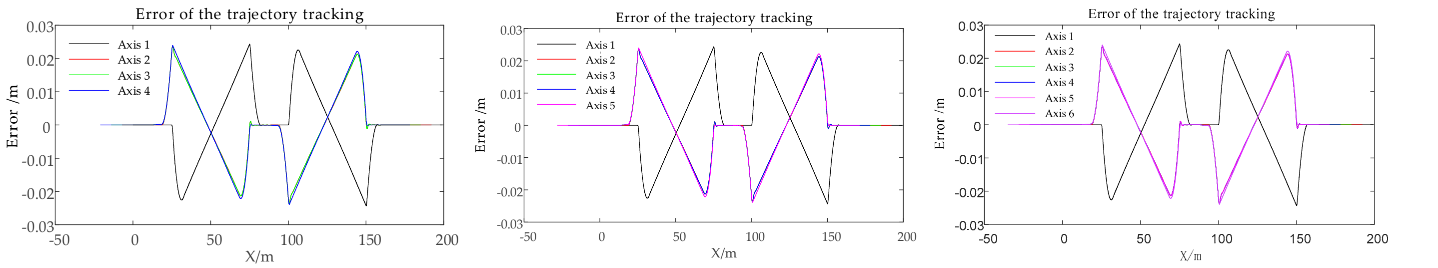

(**a**) (**b**) (**c**)

Figure 14. Trajectory-following error of the train with different configurations. (**a**) Three-carriages with four-axles train; (**b**) Four-carriages with five-axles train; (**c**) Five-carriages with six-axles train.

Under the serpentine track condition, the trajectories of each axle and the trajectory-following error of the train with different configurations are shown in Figures 15 and 16.

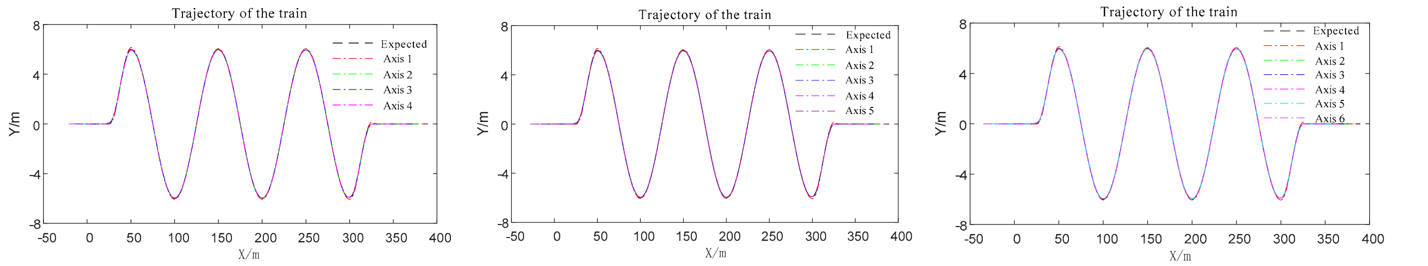

(**a**) (**b**) (**c**)

Figure 15. Trajectories of each axle of the train with different configurations. (**a**) Three-carriages with four-axles train; (**b**) Four-carriages with five-axles train; (**c**) Five-carriages with six-axles train.

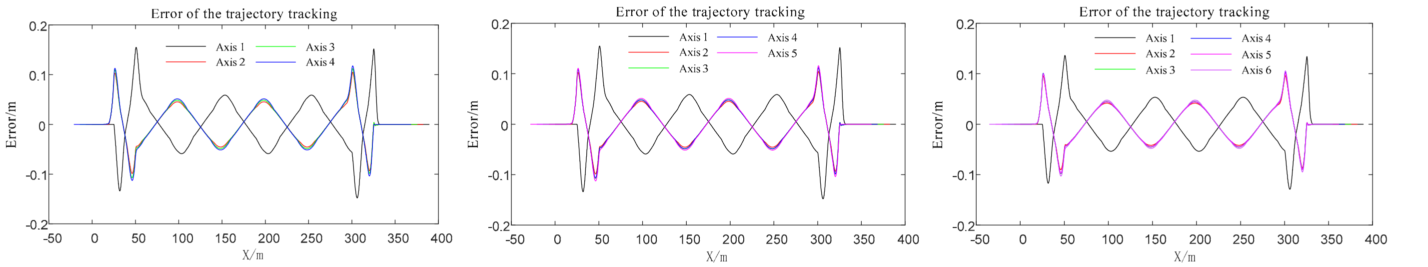

(**a**) (**b**) (**c**)

Figure 16. Trajectory-following error of the train with different configurations. (**a**) Three-carriages with four-axles train; (**b**) Four-carriages with five-axles train; (**c**) Five-carriages with six-axles train.

According to the simulation results, we can conclude that:

(1) Based on the kinematic models and the MPC-based controller established in this paper, the train with different configurations can follow the expected path. The maximum error of the trajectory following under the double lane-change condition was ± 0.025 m, while under the serpentine track condition, it was ± 0.15 m.

(2) The absolute value of the trajectory-following error of each axle was positively correlated with the curvature of the expected path. The sign of the leading car's error was opposite to that of the following carriages. The maximum error of the train with different configurations was not significantly different.

(3) When the road conditions change (such as a sudden change in the curvature of the path), the following car entered the path transition phase earlier than the leading car in position. That is to say, on the curve of the trajectory-following error, the error of the following carriage changed ahead of the path change point.

(4) The steering and/or articulation angles of the train can follow the change of the curvature of the expected path and quickly converge when the road conditions are stable. The absolute value of the articulation angle was positively correlated with the curvature of the path. The sign of the steering angle of the leading car was opposite to the articulation angle of the following carriage.

(5) The absolute value of the leading car's steering angle was significantly higher than the articulation angle of the following carriage when passing the same position. At the same time, except for the leading car, the articulation angle of the carriage increased to a certain extent compared to the preceding one when passing the same position.

4.3. The Influences of Velocity and Length of Carriage on the Controlled Variables

According to the simulation results, the articulation angle of the carriage increased compared to the preceding one under different road conditions with different configurations of the train.

To analyze the influences of velocity and length of carriage on the articulation angle, we calculated the articulation angles of the train with different lengths of carriage and at different speeds. The experimental train was a five-carriage with six-axles train. We set the speed of the train to 3 m/s, 5 m/s, and 10 m/s and set the length of the carriage to 3 m, 5 m, and 7 m, respectively.

The curve was obtained by fitting the maximum articulation angle of the different carriages passing through the same position (See Figure 17). To compare the increment of different axles with the different velocities and lengths of the carriage, t_0 was recorded as the starting time. The fitting results are shown in Figure 18.

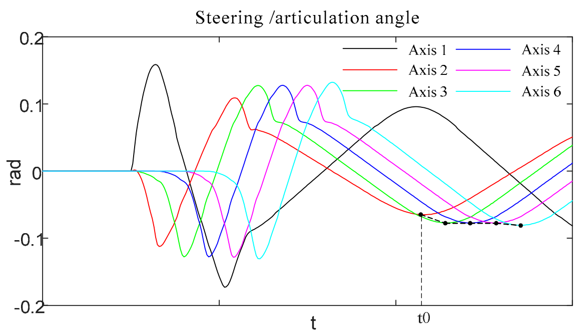

Figure 17. Steering angle/articulation angles.

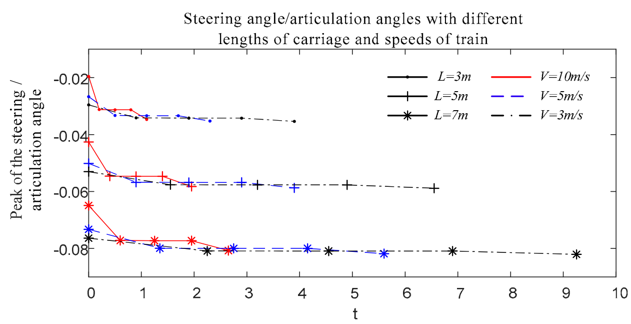

Figure 18. Steering angle and/or articulation angles with different lengths of carriage and under different speeds.

According to the simulation results, we can conclude that:

(1) Under the same road conditions, the length of the carriage affected the amplitude of the train's articulation angle. The longer the carriage, the greater the amplitude of the articulation angle.

(2) With the same carriage's length, the velocity affected the difference in the articulation angle between different axles. The greater the velocity, the greater the difference between the adjacent axles.
(3) Except for the head cab, the articulation angles of different carriages showed a gradually increasing trend from front to back. The difference between the articulation angles of the adjacent cars at the ends was the largest.
(4) Since the articulation angle of the following carriage increased compared with the preceding car, we can conclude that when an MPC controller is adopted, there is an upper limit for the number of carriages under different road conditions. When the articulation angle of the trailing car reached the maximum, if we continued to increase the number of carriages, the control force of the rear cars was insufficient and lead to the tail cars derailing.

According to the experimental results, with the same road conditions and speed, the longer the carriage's length, the fewer the maximum number of carriages.

Furthermore, in the process of actual operation, in order to reduce the impact of the modern urban bus on other urban road vehicles, avoid vehicle collisions, and improve driving safety, follow-up research will require that the author use the state information of the surrounding environment and other vehicles' speed, acceleration, and relative position, as well as comprehensively considering factors such as road vehicle traffic efficiency and obstacle avoidance, to establish a behavioral decision-making model that can generate vehicle driving decision-making instructions to determine the feasible motion state and trajectory feasible region of the vehicle in real time. Secondly, follow-up research should consider variables such as ride comfort and traffic efficiency; optimal control theory should be used to select the optimal driving trajectory from a limited set of paths; and the optimal driving trajectory should be utilized as a reference trajectory and entered into the execution module. Finally, the model predictive control algorithm described in this paper should be used as the execution module to track the optimal driving trajectory so as to realize the safe operation of modern urban buses on urban roads 5.

5. Conclusions and Further Discussion

In this paper, we proposed a generic framework that allowed for the rapid building of kinematic models for a new type of modern urban bus. By introducing the MPC model, a trajectory tracking controller for a multi-articulated vehicle with an arbitrary number of carriages was designed, and the influences of the number of carriages, velocity, and length of carriage on the trajectory tracking were further analyzed.

Through the simulation under double lane-change and serpentine track conditions, the results show that, based on the kinematic models and MPC-based controller established in this paper:

(1) The train with different configurations can follow the expected path within a small trajectory following error under different road conditions.
(2) The steering and/or articulation angles of the train can follow the change of the curvature of the expected path and quickly converge when the road conditions are stable. The absolute value of the articulation angle was positively correlated with the curvature of the path.
(3) Under the same road condition, the length of the carriage affected the amplitude of the train's articulation angle. The longer the carriage, the greater the amplitude of the articulation angle.
(4) With the same carriage's length, the velocity affected the difference in the articulation angle between different axles. The greater the velocity, the greater the difference between the adjacent axles.
(5) Except for the head cab, the articulation angles of different carriages showed a gradually increasing trend from front to back.

It can be inferred that, when determining the number of carriages for a configurable multi-articulated urban bus, we need to consider the curvature of the path, the speed of the train, the length of the carriage, and a safety redundancy to ensure that the train follows the desired path.

In this paper, we simulated the increase of the articulation angles of carriages under the stable road condition and did not conduct a comparative analysis in the transition phase between different road conditions. According to the current simulation results, in the transition phase the increase of the articulation angles of carriages was greater than that in the case of stable road conditions. Subsequent comparative analysis can be further carried out that will help us determine the maximum number of theoretical articulated carriages in actual situations.

Author Contributions: Methodology, L.S.; Resources, L.Z.; Writing—original draft, L.S.; Writing—review & editing, L.Z.; Project administration, L.Z. All authors have read and agreed to the published version of the manuscript.

Funding: This research was funded by [The Fundamental Research Funds for the Central Universities] grant number [2021YJS154].

Conflicts of Interest: The authors declare no conflict of interest.

References

1. Lei, Y.; Huang, C.F. Literature review and management expectation on the alleviating urban traffic congestion. *China Transp. Rev.* **2018**, *40*, 8–11.
2. Michalet, M.M. Modular approach to compact low-speed kinematic modelling of multi-articulated urban buses for motion algorithmization purposes. In Proceedings of the 2019 IEEE Intelligent Vehicles Symposium, Paris, France, 9–12 June 2019.
3. Odhams, A.M.C.; Roebuck, R.L.; Jujnovich, B.A.; Cebon, D. Active steering of a tractor-semi-trailer. *Proc. Inst. Mech. Eng. Part D J. Automob. Eng.* **2011**, *225*, 847–869. [CrossRef]
4. Meng, Y.; Gan, X.; Bai, G.X. Path following control of underground mining articulated vehicle based on the preview control method. *Chin. J. Eng.* **2019**, *41*, 662–671.
5. Rimmer, A.J.; Cebon, D. Implementation of reversing control on a doubly articulated vehicle. *J. Dyn. Syst. Meas. Control* **2017**, *139*, 061011. [CrossRef]
6. Ljungqvist, O.; Evestedt, N.; Axehill, D.; Cirillo, M.; Pettersson, H. A path planning and path-following control framework for a general 2-trailer with a car-like tractor. *J. Field Robot.* **2019**, *36*, 1345–1377. [CrossRef]
7. Michałek, M.M. Trailer-Maneuverability in N-Trailer Structures. *IEEE Robot. Autom. Lett.* **2020**, *5*, 5105–5112. [CrossRef]
8. Xiong, L.; Yang, X.; Zhuo, G.; Leng, B.; Zhang, R. A review of the development status of motion control for unmanned vehicles. *Chin. J. Mech. Eng.* **2020**, *56*, 127–143.
9. Bai, G.; Luo, W.; Liu, L.; Meng, Y.; Gu, Q.; Li, K. Research status and progress of path-following control of mine-used articulated vehicles. *Chin. J. Eng. Sci.* **2021**, *43*, 193–204.
10. Li, S.; Liu, Y.; Qu, X. Model Controlled Prediction: A Reciprocal Alternative of Model Predictive Control. *IEEE/CAA J. Autom. Sin.* **2022**, *9*, 1107–1110. [CrossRef]
11. Yamaguchi, H.; Mori, M.; Kawakami, A. Control of a Five-axle, Three-steering Coupled-vehicle System and its Experimental Verification. *IFAC Proc. Vol.* **2011**, *44*, 12976–12984. [CrossRef]
12. Astolfi, A.; Bolzern, P.; Locatelli, A. Path-tracking of a tractor-trailer vehicle along rectilinear and circular paths: A Lyapunov-based approach. *IEEE Trans. Robot. Autom.* **2004**, *20*, 154–160. [CrossRef]
13. Sampei, M.; Tamura, T.; Kobayashi, T. and Shibui, N. Arbitrary path tracking control of articulated vehicles using nonlinear control theory. *IEEE Trans. Control Syst. Technol.* **1995**, *3*, 125–131. [CrossRef]
14. Wang, W.; Zhao, Y.; Xu, J.; Liu, W. Research on Vehicle Path Tracking Based on Fuzzy Control. *China Mech. Eng.* **2014**, *25*, 2532–2538.
15. Zhang, G.; Li, J.; Liu, C. and Zhang, W. A robust fuzzy speed regulator for unmanned sailboat robot via the composite ILOS guidance. *Nonlinear Dyn.* **2022**, *110*, 2465–2480. [CrossRef]
16. Zhang, G.; Liu, S.; Zhang, X.; Zhang, W. Event-Triggered Cooperative Formation Control for Autonomous Surface Vehicles Under the Maritime Search Operation. *IEEE Trans. Intell. Transp. Syst.* **2022**, *23*, 21392–21404. [CrossRef]
17. Zhao, H. Research on Dynamics Analysis and Path Tracking Control Method of Electric Articulated Tracked Vehicles. Ph.D. Thesis, Jilin University, Changchun, China, 2018.
18. Meng, Y.; Wang, Y.; Gu, Q.; Bai, G. LQR-GA Path Tracking Control of Articulated Vehicles Based on Foresight Pose Information. *J. Agric. Mach.* **2018**, *49*, 375–384.
19. Nie, Z.; Zong, C.; Yang, X.; Gao, J.; Zhang, K. Active Steering Control Strategy for Medium and High-Speed Heavy-duty Semi-trailer Trailers with Mode Switching. *J. Chongqing Univ.* **2017**, *40*, 78–89.
20. Wang, L. *Model Predictive Control System Design and Implementation Using MATLAB®*; Springer Science & Business Media: Berlin/Heidelberg, Germany, 2009.

21. Wu, T.; Hung, J.Y. Path following for a tractor-trailer system using model predictive control. In Proceedings of the SoutheastCon 2017, Concord, NC, USA, 30 March–2 April 2017; pp. 1–5.
22. Lin, Y.; Yin, G.; Liang, Q.; Wang, L. Cross-line-turn path tracking of intelligent agricultural vehicle based on MPC in standard orchard. In Proceedings of the 2018 Chinese Control and Decision Conference (CCDC), Shenyang, China, 09–11 June 2018; pp. 4786–4791.
23. Yue, M.; Hou, X.; Yang, L. An efficient trajectory tracking control for tractor-trailer vehicle system. In Proceedings of the 2017 36th Chinese Control Conference (CCC), Dalian, China, 26–28 July 2017; pp. 546–551.
24. *GB/T6323-2014*; Controllability and Stability Test Procedure for Automobile. Standardization Administration: Beijing, China, 2014.
25. Liu, Z.; Yue, M.; Guo, L.; Zhang, L. Trajectory planning and robust tracking control for a class of active articulated tractor-trailer vehicle with on-axle structure. *Eur. J. Control* **2020**, *54*, 87–98. [CrossRef]